Steady-State Kinetics and Mechanism of LpxD, the *N*-Acyltransferase of Lipid A Biosynthesis[†]

Craig M. Bartling and Christian R. H. Raetz*

Department of Biochemistry, Duke University Medical Center, P.O. Box 3711, Durham, North Carolina 27710

Received February 10, 2008; Revised Manuscript Received March 12, 2008

ABSTRACT: LpxD catalyzes the third step of lipid A biosynthesis, the (*R*)-3-hydroxymyristoyl-acyl carrier protein (*R*-3-OHC_{14}-ACP)-dependent N-acylation of UDP-3-*O*-[(*R*)-3-hydroxymyristoyl]-α-D-glucosamine [UDP-3-*O*-(*R*-3-OHC_{14})-GlcN]. We have now overexpressed and purified *Escherichia coli* LpxD to homogeneity. Steady-state kinetics suggest a compulsory ordered mechanism in which *R*-3-OHC_{14}-ACP binds prior to UDP-3-*O*-(*R*-3-OHC_{14})-GlcN. The product, UDP-2,3-diacylglucosamine, dissociates prior to ACP; the latter is a competitive inhibitor against *R*-3-OHC_{14}-ACP and a noncompetitive inhibitor against UDP-3-*O*-(*R*-3-OHC_{14})-GlcN. UDP-2-*N*-[(*R*)-3-Hydroxymyristoyl]-α-D-glucosamine, obtained by mild base hydrolysis of UDP-2,3-diacylglucosamine, is a noncompetitive inhibitor against both substrates. Synthetic (*R*)-3-hydroxylauroyl-methylphosphopantetheine is an uncompetitive inhibitor against *R*-3-OHC_{14}-ACP and a competitive inhibitor against UDP-3-*O*-(*R*-3-OHC_{14})-GlcN, but (*R*)-3-hydroxylauroyl-methylphosphopantetheine is also a very poor substrate. A compulsory ordered mechanism is consistent with the fact that *R*-3-OHC_{14}-ACP has a high binding affinity for free LpxD whereas UDP-3-*O*-(*R*-3-OHC_{14})-GlcN does not. Divalent cations inhibit *R*-3-OHC_{14}-ACP-dependent acylation but not (*R*)-3-hydroxylauroyl-methylphosphopantetheine-dependent acylation, indicating that the acidic recognition helix of *R*-3-OHC_{14}-ACP contributes to binding. The F41A mutation increases the K_M for UDP-3-*O*-(*R*-3-OHC_{14})-GlcN 30-fold, consistent with aromatic stacking of the corresponding F43 side chain against the uracil moiety of bound UDP-GlcNAc in the X-ray structure of *Chlamydia trachomatis* LpxD. Mutagenesis implicates *E. coli* H239 but excludes H276 as the catalytic base, and neither residue is likely to stabilize the oxyanion intermediate.

Lipid A is the hydrophobic moiety of lipopolysaccharide (LPS),[1] which constitutes the outer leaflet of the outer membrane of most Gram-negative bacteria (*1*−*3*). The lipid A moiety of LPS is usually required for bacterial growth (*3, 4*) and is a potent activator of the mammalian innate immune system via the TLR4−MD-2 complex (*5, 6*). Overproduction of cytokines due to excessive stimulation of the TLR4−MD-2 complex may occur during severe Gram-negative infections and may contribute to the life-threatening complications of septic shock (*7, 8*).

The Kdo_2−lipid A substructure of *Escherichia coli* LPS is synthesized by a conserved system of nine constitutive enzymes (Figure 1A) (*3*). LpxD catalyzes the third reaction in this scheme, the (*R*)-3-hydroxymyristoyl-acyl carrier protein (*R*-3-OHC_{14}-ACP)-dependent N-acylation of UDP-3-*O*-[(*R*)-3-hydroxymyristoyl]-α-D-glucosamine [UDP-3-*O*-(*R*-3-OHC_{14})-GlcN] (*9*) (Figure 1A). Although essential for growth and an excellent target for the design of new antibiotics (*9*), LpxD is one of the least characterized enzymes in the pathway. Kelly and Raetz identified the function of LpxD and reported a quantitative assay, which demonstrated high selectivity of *E. coli* LpxD (EcLpxD) for the presence of the (*R*)-3-OH moiety and 14 carbons in the acyl-ACP donor substrate (*9*). Apparent K_M values in cell-free extracts for UDP-3-*O*-(*R*-3-OHC_{14})-GlcN and *R*-3-OHC_{14}-ACP were reported to be 1.3 and 1.9 μM, respectively (*9*). No other functional studies of LpxD catalysis have appeared.

On the basis of its sequence, LpxD belongs to a large family of trimeric acyl- and acetyltransferases that are characterized by the presence of a left-handed parallel β helix (Lβ H) domain (*10*−*13*). This unusual secondary structure was first identified in *E. coli* LpxA (Figure 1B) (*10*). Recently, several crystal structures of *Chlamydia trachomatis* LpxD (CtLpxD) were reported by Buetow et al. (*14*). Complex I, determined at 2.2 Å (*14*), was crystallized in the presence of 25 mM UDP-GlcNAc; it also contained extraneous bound palmitate molecules (Figure 1C). The structure of Complex II (not shown in Figure 1) was determined at 3.1 Å resolution (*14*). This sample was prepared in the presence of 100 mM UDP-GlcNAc and likewise contained bound free fatty acids (*14*). All CtLpxD structures revealed the same Lβ H fold and trimeric archi-

[†] This research was supported by NIH Grant GM-51310 to C.R.H.R.

* To whom correspondence should be addressed. Phone: (919) 684-3384. Fax: (919) 684-8885. E-mail: raetz@biochem.duke.edu.

[1] Abbreviations: ACP, acyl carrier protein; Bis-Tris, 2,2-bis(hydroxymethyl)-2,2′,2″-nitrilotriethanol; CMC, critical micelle concentration; EcLpxD, *Escherichia coli* LpxD; CtLpxD, *Chlamydia trachomatis* LpxD; Hepes, 4-(2-hydroxyethyl)-1-piperazineethanesulfonic acid; Lβ H, left-handed parallel β helix; LPS, lipopolysaccharide; *R*-3-OHC_{14}-ACP, (*R*)-3-hydroxymyristoyl-acyl carrier protein; SDS−PAGE, sodium dodecyl sulfate−polyacrylamide gel electrophoresis; UDP-3-*O*-(*R*-3-OHC_{14})-GlcN, UDP-3-*O*-[(*R*)-3-hydroxymyristoyl]-α-D-glucosamine; UDP-2-*N*-(*R*-3-OHC_{14})-GlcN, UDP-2-*N*-[(*R*)-3-hydroxymyristoyl]-α-D-glucosamine.

10.1021/bi800240r CCC: $40.75
Published on Web 04/19/2008

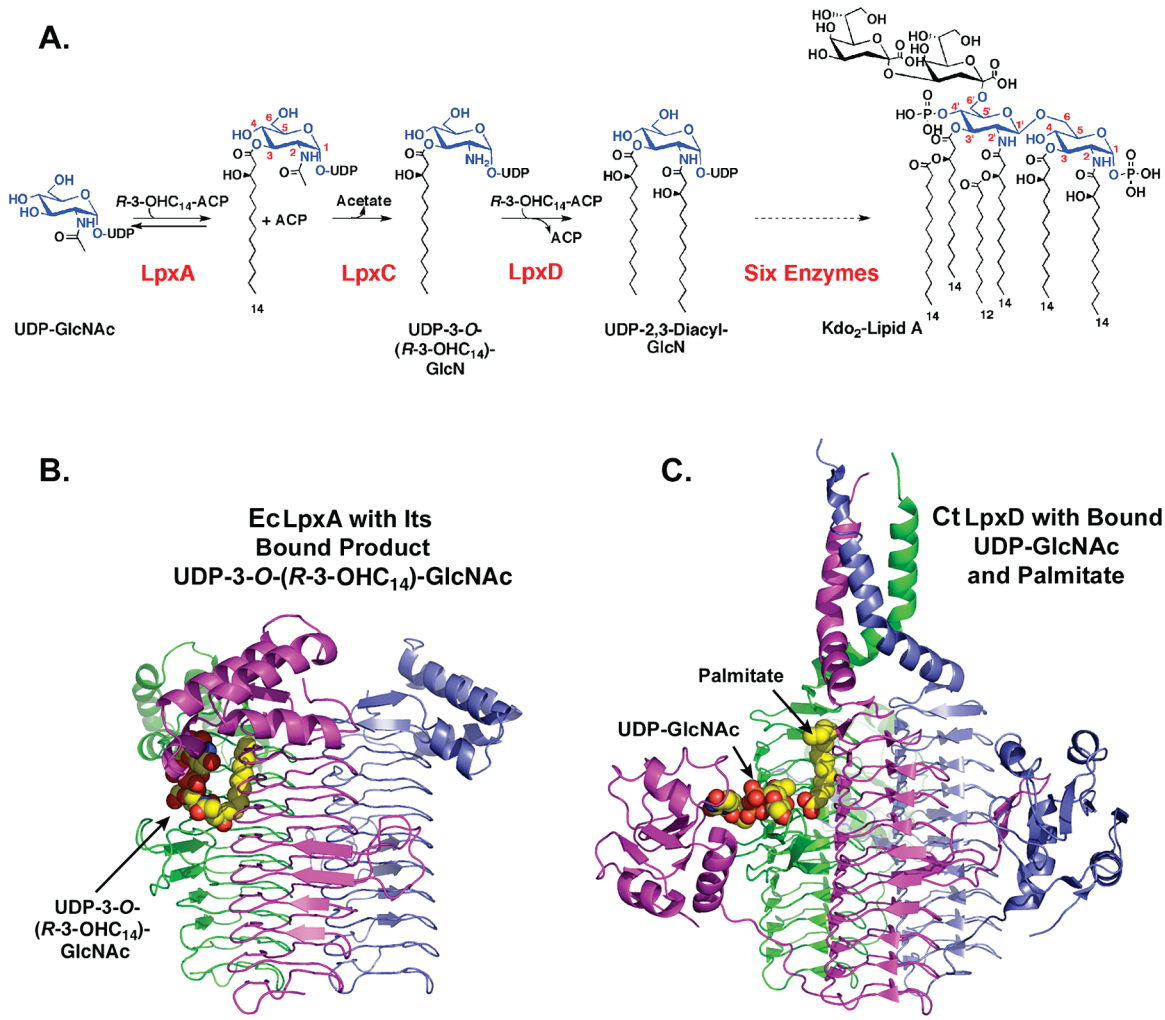

FIGURE 1: Role of LpxD in *E. coli* lipid A biosynthesis. (A) LpxD is the third enzyme in the lipid A pathway. *E. coli* LpxD catalyzes the *R*-3-OHC$_{14}$-ACP-dependent N-acylation of UDP-3-*O*-(*R*-3-OHC$_{14}$)-GlcN to generate UDP-2,3-diacylglucosamine and ACP (*9*). Six additional enzymes are required to make Kdo$_2$−lipid A, the minimal LPS substructure required for growth in most Gram-negative bacteria (*3*). (B) Crystal structure at 1.75 Å of *E. coli* LpxA with its bound product UDP-3-*O*-[(*R*)-3-hydroxymyristoyl]-α-D-*N*-acetylglucosamine (*17*). (C) Crystal structure of LpxD with bound UDP-GlcNAc and free fatty acid, modeled as palmitate (Complex I) (*14*). Each subunit of the LpxA or LpxD homotrimer is colored green, magenta, or slate. In the bound ligands, carbon is colored yellow, nitrogen blue, oxygen red, and phosphorus orange.

tecture seen with LpxA (Figure 1B,C) (*14*). Although no assays were reported, Buetow et al. (*14*) proposed a mechanism for LpxD involving nucleophilic attack by the N atom of UDP-3-*O*-(*R*-3-OHC$_{14}$)-GlcN on the thioester carbonyl moiety of acyl-ACP. Given their general locations within the active site region, both H247 and H284 of CtLpxD were proposed to activate the N atom of the acceptor UDP-3-*O*-(*R*-3-OHC$_{14}$)-GlcN and/or stabilize the oxyanion intermediate (*14*). In fact, all the enzymes in the LβH acyltransferase class contain at least one essential histidine residue thought to function as the general base (*13*). In LpxA, the H125A mutation abolishes activity (*15*), consistent with the fact that Nε2 of H125 is within hydrogen bonding distance of the 3-OH group of bound UDP-GlcNAc or UDP-3-*O*-(*R*-3-hydroxymyristoyl)-GlcNAc (*16, 17*).

Many acyltransferases in the LβH family are thought to operate by sequential mechanisms. For example, serine acetyltransferase has an ordered sequential mechanism in which acetyl-CoA binds prior to L-serine and *O*-acetylserine dissociates before coenzyme A (*18*). Galactoside acetyltransferase (*19*), maltose acetyltransferase (*20*), and LpxA (*21*) likewise exhibit sequential mechanisms, but in the case of LpxA, the binding order is unknown (*21*). Glycerol-3-phosphate acyltransferase of squash chloroplasts, a soluble non-LβH acyltransferase, displays an ordered sequential mechanism in which the acyl-ACP donor binds first (*22*).

We now present the first steady-state kinetic analysis of EcLpxD. We have purified untagged EcLpxD and an active N-terminally His$_6$-tagged LpxD variant to near homogeneity. On the basis of the steady-state kinetics and the effects of several inhibitors, we suggest a compulsory ordered mechanism in which *R*-3-OHC$_{14}$-ACP binds prior to UDP-3-*O*-(*R*-3-OHC$_{14}$)-GlcN and UDP-2,3-diacylglucosamine dissociates prior to ACP (Scheme 1). Direct binding studies with the physiological LpxD substrates, *R*-3-OHC$_{14}$-ACP and UDP-3-*O*-(*R*-3-OHC$_{14}$)-GlcN (Figure 1A), provide independent support for this order of events. Site-directed mutagenesis and kinetic analyses of selected mutants support a chemical mechanism in which EcLpxD H239 (CtLpxD H247) is the catalytic base and EcLpxD H276 (CtLpxD H284) participates in substrate binding. This conclusion was not clear from the crystal structures of CtLpxD Complexes I and II (*14*), which were determined in the presence of bound

Scheme 1: A Possible Ordered Sequential Kinetic Mechanism for LpxD[a]

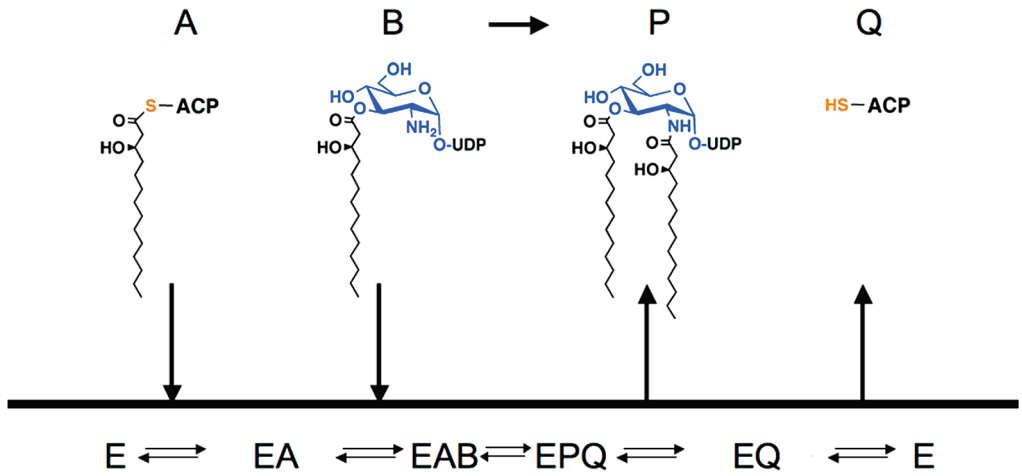

[a] Abbreviations: E, LpxD; A, *R*-3-OHC$_{14}$-ACP; B, UDP-3-*O*-(*R*-3-OHC$_{14}$)-GlcN; P, UDP-2,3-diacylglucosamine; and Q, ACP.

UDP-GlcNAc and free fatty acids (Figure 1C), but not with the physiological CtLpxD ligands.

MATERIALS AND METHODS

Reagents and Materials. [α-^{32}P]UTP was purchased from NEN DuPont (Boston, MA), and oligonucleotides were purchased from MWG Biotech (High Point, NC). (*R*)-3-Hydroxylauroyl-methylphosphopantetheine was synthesized by Avanti Polar Lipids (Alabaster, AL). All other chemicals were purchased from Sigma Chemical Co. (St. Louis, MO) or prepared as described below. G-50 spin columns were purchased from GE Healthcare (Piscataway, NJ), and C_{18} Sep-Pak columns were purchased from Waters (Milford, MA). Substrates and reagents, such as *R*-3-OHC$_{14}$-ACP, *R*/*S*-3-hydroxylauroyl-ACP (*9*), [α-^{32}P]UDP-GlcNAc (*9*), and [α-^{32}P]UDP-3-*O*-(*R*-3-OHC$_{14}$)-GlcN (*9, 23*), were prepared by minor modifications of published methods (see the Supporting Information).

LpxD Assay. The LpxD assay was carried out as previously reported (*9*). Unless otherwise noted, the 10 μL assay mixture contained 40 mM Hepes (pH 7.5), 0.02 mg/mL BSA, 0.1 nM pure wild-type *E. coli* LpxD (or up to 10 nM mutant LpxD), [α-^{32}P]UDP-3-*O*-(*R*-3-OHC$_{14}$)-GlcN (4 μM, 0.005−0.04 μCi/μL), and 6 μM *R*-3-OHC$_{14}$-ACP. The concentration of UDP-3-*O*-(*R*-3-OHC$_{14}$)-GlcN was determined using the UDP extinction coefficient of 9900 M^{-1} cm^{-1} (*24*). The components were equilibrated at 30 °C, and the reaction was started by addition of enzyme. Time points were taken by spotting 1 μL portions of the reaction mixture onto a silica thin layer chromatography plate. After drying under a cold air stream, plates were developed with a chloroform/methanol/water/acetic acid solvent (25:15:4:2, v/v/v/v). After removal of the solvent, the plates were exposed overnight to a Molecular Dynamics PhosphorImager Screen. The percent of the [α-^{32}P]UDP-3-*O*-(*R*-3-OHC$_{14}$)-GlcN converted to [α-^{32}P]UDP-2,3-diacylglucosamine was quantified with ImageQuant.

Cloning, Expression, and Purification of EcLpxD. Both untagged EcLpxD and His$_6$-EcLpxD were prepared and purified to homogeneity (see the Supporting Information). Cells were grown on LB broth or LB agar (*25*), supplemented with antibiotics as indicated, and protein concentrations were determined using the bicinchoninic acid method (*26*).

Site-Directed Mutagenesis. LpxD point mutants were constructed using pNH6LpxD as the template, and the mutants were overexpressed in the same manner as described for the untagged protein. The various His$_6$-tagged LpxDs were purified from cell-free extracts derived from 125 mL cultures. The LpxD derivatives were purified over a 1 mL Ni-NTA column (Qiagen) washed with 40 mM potassium phosphate (pH 8.0) containing 250 mM NaCl and 20 mM imidizole. The desired LpxDs were eluted from the column in 40 mM potassium phosphate (pH 8.0) containing 250 mM NaCl and 150 mM imidizole. PD-10 columns (GE-Healthcare) were used to exchange the LpxDs eluted from the Ni-NTA columns into 10 mM potassium phosphate (pH 7.0) containing 20% glycerol and 200 mM NaCl. Proteins were concentrated to 1−10 mg/mL and stored at −80 °C. The specific activity and Michaelis−Menten constants of the purified N-terminally His$_6$-tagged LpxD were the same as for the pure untagged protein (data not shown). However, a C-terminally His$_6$-tagged LpxD construct was 50 times less active than the native protein, when assayed in cell-free extracts, even though the extent of protein expression, as judged by SDS−PAGE analysis, was not diminished (data not shown).

Bisubstrate Kinetics. Bisubstrate kinetic analysis was performed by titrating one substrate from 0.5 to 8 μM while holding the other substrate constant at 0.5, 1, 2, 4, or 8 μM. Equations for a ping-pong (eq 1) and a sequential (eq 2) reaction mechanism were fit globally (GraFit software[2]) using a least-squares nonlinear approach:

$$v = V_m AB/(K_{Ma}B + K_{Mb}A + AB) \quad (1)$$

$$v = V_m AB/(K_{Ma}B + K_{Mb}A + K_{ia}K_{Mb} + AB) \quad (2)$$

where *A* and *B* are the concentrations of substrates A and B, respectively, K_{Ma} is the K_M for substrate A, K_{Mb} is the K_M for substrate B, and K_{ia} is the dissociation constant for substrate A. V_m is the maximal velocity.

Inhibition Kinetics. To determine inhibition patterns for ACP, UDP-2-*N*-(*R*-3-OHC$_{14}$)-GlcN, and (*R*)-3-hydroxylauroyl-methylphosphopantetheine, one substrate was varied

[2] Leatherbarrow, R. J. (2001) *GraFit*, version 5, Erithacus Software, Ltd., Horley, U.K.

from approximately 5-fold below to 5-fold above the K_M while the other substrate was held constant at 2-fold above the K_M at fixed concentrations of the inhibitor (0−5-fold above the K_i). Nonlinear least-squares fits (GraFit software[2]) of the equations for competitive (eq 3), uncompetitive (eq 4), or noncompetitive (eq 5) inhibition were used to evaluate the data:

$$v = (V_m S)/[K_M(1 + I/K_{ic}) + S] \quad (3)$$

$$v = (V_m S)/[K_M + S(1 + I/K_{iu})] \quad (4)$$

$$v = (V_m S)/[K_M(1 + I/K_{in}) + S(1 + I/K_{in})] \quad (5)$$

K_{ic} is the inhibition constant for a competitive inhibitor with respect to substrate S, K_{iu} is the inhibition constant for an uncompetitive inhibitor with respect to substrate S, and K_{in} is the inhibition constant for a noncompetitive inhibitor with respect to substrate S. Data were also evaluated by fitting to a mixed inhibition model (where the first K_{in} in eq 5 does not equal the second), but this approach did not yield the lowest χ^2.

Binding Assays. A modified procedure of Penefsky was used to determine dissociation constants for each substrate (*27, 28*). Either [α-^{32}P]UDP-3-*O*-(*R*-3-OHC$_{14}$)-GlcN (24 nM) or nonradioactive *R*-3-OHC$_{14}$-ACP (5 nM) was incubated with pure LpxD (from 0 to 160 μM as indicated) in 20 μL for 15 min at 30 °C in 40 mM Hepes (pH 7.5). EDTA (1 mM) was included in the incubations containing *R*-3-OHC$_{14}$-ACP to prevent interactions with residual divalent cations. At concentrations of ≤1 mM, EDTA has no effect on LpxD activity (data not shown). G-50 spin columns (GE Healthcare) were supplied in 10 mM Tris-HCl (pH 8.0) and 1 mM EDTA, and they were equilibrated by centrifugation at 2000*g* for 1 min. The binding mixture was then applied, and the column was centrifuged again for 1 min. For the [α-^{32}P]UDP-3-*O*-(*R*-3-OHC$_{14}$)-GlcN binding assays, the counts in the run-through, a measure of the binding of [α-^{32}P]UDP-3-*O*-(*R*-3-OHC$_{14}$)-GlcN to LpxD, were quantified and compared to the total counts loaded onto the column. Approximately 5% of the total counts of [α-^{32}P]UDP-3-*O*-(*R*-3-OHC$_{14}$)-GlcN loaded on the columns emerged in the run-through in the absence of LpxD. The fraction of the [α-^{32}P]UDP-3-*O*-(*R*-3-OHC$_{14}$)-GlcN bound to LpxD at various concentrations of LpxD was then determined using eq 6.

$$[EL]/[L]_{total} = [(ligand)_{eluate} - (ligand)_{bckgrnd}]/[(ligand)_{total} - (ligand)_{bckgrnd}] \quad (6)$$

Because the *R*-3-OHC$_{14}$-ACP substrate was not radiolabeled, the amount of *R*-3-OHC$_{14}$-ACP bound to LpxD ([EL] in eq 6) in the absence of acceptor substrate was determined by diluting 5 μL of the run-through into a 10 μL assay mixture containing 5 nM [α-^{32}P]UDP-3-*O*-(*R*-3-OHC$_{14}$)-GlcN (approximately 2-fold excess of the maximum concentration of *R*-3-OHC$_{14}$-ACP) and ≥1 μM LpxD (single-turnover conditions). The concentration of the [α-^{32}P]UDP-2,3-diacylglucosamine product formed under these conditions was directly proportional to the concentration of *R*-3-OHC$_{14}$-ACP in the run-through. Concentrations were normalized to a control assay mixture that contained 2.5 nM *R*-3-OHC$_{14}$-ACP. Under these conditions, the LpxD reaction goes to completion within seconds, and no reverse reaction occurs (data not shown). Approximately 5−10% of the total *R*-3-OHC$_{14}$-ACP loaded onto the G-50 spin column emerges in the run-through in the absence of LpxD, and this background was subtracted. Equation 7 was fit to the data to determine dissociation constants for both ligands (*29*).

$$[EL]/[L]_{total} = 1/(1 + K_d/[E]_{total}) \quad (7)$$

Steady-State Kinetic Constants of Wild-Type and Mutant EcLpxD. To determine the apparent k_{cat} and K_M for wild-type and mutant LpxDs, one substrate was varied from approximately 5-fold below to 5-fold above the K_M while the other substrate was held constant 2-fold above the K_M. *R*-3-OHC$_{14}$-ACP curves were used to determine k_{cat} in all cases. To determine k_{cat} and K_M, eq 8 was fit to the data using KaleidaGraph (Synergy Software, Reading, PA):

$$v = (k_{cat}E_0 S)/(K_M + S) \quad (8)$$

Inhibition by Divalent Cations. To study the inhibition of EcLpxD by Ca^{2+}, Mg^{2+}, Na^+, or K^+ ions, the chloride salt of each cation was titrated into the LpxD assay system from 0 to 10 mM. Inhibition data were fit to eq 9, using KaleidaGraph:

$$v_i/v_0 = 1/[1 + (I/IC_{50})^h] \quad (9)$$

In this case, v_i is the inhibited velocity, v_0 the velocity without added inhibitor, I the concentration of the cation, IC_{50} the concentration of I when $v_i/v_0 = 0.5$, and h the Hill coefficient, which was always in the range of 0.7−1.3.

RESULTS

Purification of Untagged EcLpxD. EcLpxD activity was overexpressed approximately 1000-fold relative to a vector control (based on specific activity measurements) by inducing the *lpxD* gene cloned behind the T7 promoter of the pDC015-1 plasmid harbored in *E. coli* Rosetta (DE3)/pLysS. Purification to greater than 95% homogeneity of the untagged protein was achieved by a combination of dye affinity (Green-19), anion exchange (Q-Sepharose), and gel filtration (Sephadex-G200) chromatography. Figure 1 of the Supporting Information shows the analysis by SDS−PAGE of samples from each step of the purification. In a typical preparation derived from an induced 4 L culture, a 3.4-fold purification (Table 1) was required to achieve near homogeneity (∼15 mg of pure protein per liter), as judged by SDS−PAGE. LpxD eluted as a single symmetrical peak from a Sephadex-G200 column at an elution volume consistent with a mass of 108 kDa, indicating that the enzyme is a homotrimer in aqueous solution. Electrospray ionization time-of-flight mass spectrometry gave a subunit molecular mass of 35880 Da, in good agreement with the expected molecular mass of 35881 Da for LpxD (untagged LpxD with the P2A substitution).

Steady-State Kinetics of EcLpxD. LpxD catalyzes the transfer of the (*R*)-3-hydroxymyristoyl chain from *R*-3-OHC$_{14}$-ACP to UDP-3-*O*-(*R*-3-OHC$_{14}$)-GlcN to make UDP-2,3-diacylglucosamine and ACP (Figure 1). Like LpxA and LpxC, LpxD does not require the presence of a detergent for catalytic activity because the critical micelle concentrations of its substrates are likely to be >100 μM (well above their K_M values), based on studies with other monoacylated phospholipids (*30*).

Table 1: Purification of *E. coli* LpxD

step	total volume (mL)	total protein (mg)	total units (nmol/min)	specific activity (nmol min^{-1} mg^{-1})	*x*-fold purification	yield (%)
crude extract	250	692.5	1828200	2640	1	100
Green-19	139	150.1	1059800	7060	2.7	58
Q-Sepharose	10	80.3	629600	7840	3.0	34
gel filtration	5.4	64.3	571900	8900	3.4	31

To determine the order of substrate binding and product release, we first determined whether LpxD catalysis conforms to a ping-pong or a sequential mechanism (*31*). A priori, it seemed unlikely that LpxD would function through an acyl−enzyme intermediate, because no conserved cysteine or serine residues are found when diverse LpxD sequences are aligned. Initial velocity patterns for each substrate (varied from 5-fold below to 5-fold above the K_M) were determined at fixed concentrations (0.5, 1, 2, 4, and 8 μM) of the other substrate. A ping-pong (eq 1) or a sequential mechanism (eq 2) was fit to the data. The global fit of the sequential mechanism (Figure 2) was much better than that of the ping-pong mechanism (data not shown). In the double-reciprocal plots (Figure 2), the initial velocity patterns intersect to the left of the *y*-axis, clearly supporting a sequential mechanism with a V_m of 0.11 ± 0.007 μM/min, a K_{Ma} of 3.2 ± 0.6 μM, a K_{Mb} of 1.3 ± 0.2 μM, and a K_{ia} of 4.3 ± 2.6 μM, where substrate A is *R*-3-OHC$_{14}$-ACP and substrate B is UDP-3-*O*-(*R*-3-OHC$_{14}$)-GlcN, as shown in Scheme 1. A sequential mechanism implies that both substrates must bind to the enzyme in a ternary complex before catalysis can occur, but it does not distinguish ordered from random substrate binding and product dissociation.

Inhibition of EcLpxD by ACP and UDP-2-N-(R-3-OHC$_{14}$)-GlcN. Product and substrate analogue inhibition patterns were examined to determine the order of substrate binding and product dissociation (*31*). Initial velocity patterns were then assigned to a competitive (eq 3), uncompetitive (eq 4), or noncompetitive (eq 5) mode of inhibition, based on the model that yielded the best least-squares fit. In all cases, two or more experiments were performed to determine the mode of inhibition (data not shown). The representative plots

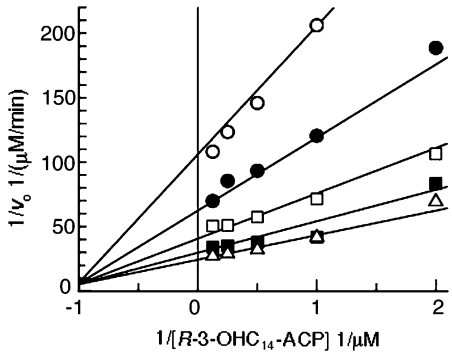

FIGURE 2: Kinetic evidence for a sequential LpxD mechanism. The plot displays the Lineweaver−Burke representation of the initial velocities as a function of substrate concentration. *R*-3-OHC$_{14}$-ACP concentrations were varied from 5-fold below to 5-fold above the K_M as shown with the UDP-3-*O*-(*R*-3-OHC$_{14}$)-GlcN concentrations held constant at 0.5 (○), 1 (●), 2 (□), 4 (■), or 8 μM (△). Nonlinear fits (displaying the lowest χ^2 values) were derived by least-squares fitting using GraFit.[2]

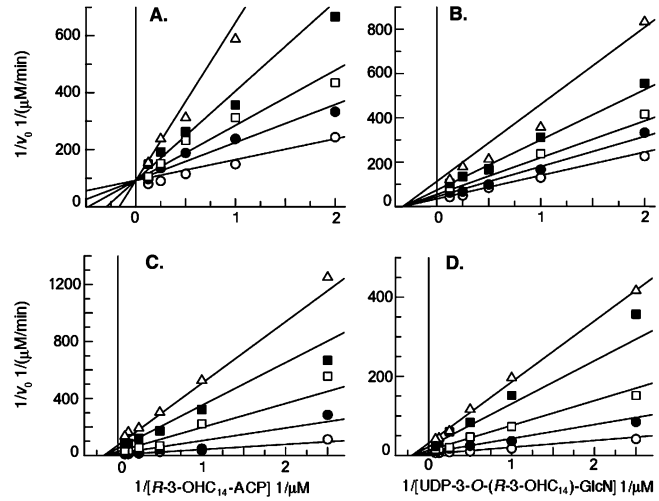

FIGURE 3: Inhibition of LpxD by ACP and UDP-2-*N*-(*R*-3-OHC$_{14}$)-GlcN. The plots display the Lineweaver−Burke representations of initial velocities as a function of substrate concentration at increasing constant concentrations of each inhibitor. Substrate concentrations were varied as shown from 5-fold below to 5-fold above the K_M with the second substrate concentration held constant 2-fold above its K_M. Nonlinear fits (displaying the lowest χ^2 values) were derived by least-squares fitting using GraFit Software.[2] ACP concentrations were held constant at 0 (○), 40 (●), 80 (□), 160 (■), or 360 μM (△). UDP-2-*N*-(*R*-3-OHC$_{14}$)-GlcN concentrations were held constant at 0 (○), 10 (●), 25 (□), 50 (■), or 75 μM (△). (A) ACP is competitive with respect to *R*-3-OHC$_{14}$-ACP. (B) ACP is noncompetitive with respect to UDP-3-*O*-(*R*-3-OHC$_{14}$)-GlcN. (C) UDP-2-*N*-(*R*-3-OHC$_{14}$)-GlcN is noncompetitive with respect to *R*-3-OHC$_{14}$-ACP (χ^2 for a competitive fit, 2.9 × 10^{-5}; χ^2 for a noncompetitive fit, 1.0 × 10^{-5}). (D) UDP-2-*N*-(*R*-3-OHC$_{14}$)-GlcN is noncompetitive with respect to UDP-3-*O*-(*R*-3-OHC$_{14}$)-GlcN (χ^2 for a competitive fit, 5.8 × 10^{-5}; χ^2 for a noncompetitive fit, 3.9 × 10^{-5}).

display the double-reciprocal (Lineweaver−Burke) representations of the best nonlinear fits derived from least-squares fitting.

As shown in panels A and B of Figure 3, ACP is a competitive inhibitor with respect to *R*-3-OHC$_{14}$-ACP with a K_{ic} of 48 ± 10 μM and a noncompetitive inhibitor with respect to UDP-3-*O*-(*R*-3-OHC$_{14}$)-GlcN with a K_{in} of 139 ± 20 μM. The data are consistent with Scheme 1, an ordered mechanism in which *R*-3-OHC$_{14}$-ACP (A) binds to LpxD (E), followed by UDP-3-*O*-(*R*-3-OHC$_{14}$)-GlcN (B). After catalysis, UDP-2,3-diacylglucosamine (P) dissociates before ACP (Q) to re-form the free enzyme (E). In this model, ACP should be competitive with respect to *R*-3-OHC$_{14}$-ACP because both bind to the free form of the enzyme. Furthermore, ACP should be noncompetitive with respect to UDP-3-*O*-(*R*-3-OHC$_{14}$)-GlcN because each binds to a different form of the enzyme (Scheme 1).

Previous studies have demonstrated that the critical micelle concentration of the LpxD product UDP-2,3-diacylglucosamine is 20 μM (*32*). To avoid issues related to micelle formation, inhibition by UDP-2,3-diacylglucosamine was not investigated. Instead, UDP-2,3-diacylglucosamine was O-deacylated with a mild base at the GlcN 3-position to form the product substructure UDP-2-*N*-(*R*-3-OHC$_{14}$)-GlcN, which should have a CMC of >100 μM. As shown in panels C and D of Figure 3, UDP-2-*N*-(*R*-3-OHC$_{14}$)-GlcN is a noncompetitive inhibitor with respect to both substrates with a K_{in} of 6.0 ± 1.1 μM against *R*-3-OHC$_{14}$-ACP and a K_{in} of 9.4 ± 0.8 μM against UDP-3-*O*-(*R*-3-OHC$_{14}$)-GlcN. This is consistent with Scheme 1 in which UDP-2,3-diacylglu-

Table 2: LpxD Reactivity and Structures of Various Acyl Donors

acyl donor (10 μM)	specific activity (nmol min^{-1} mg^{-1})
R-3-hydroxymyristoyl-ACP	15.1×10^3
R-3-hydroxylauroyl-ACP[a]	1.46×10^3
(*R*)-3-hydroxylauroyl-methylphosphopantetheine	0.010×10^3

[a] Prepared as the 20 μM *R*/*S* mixture.

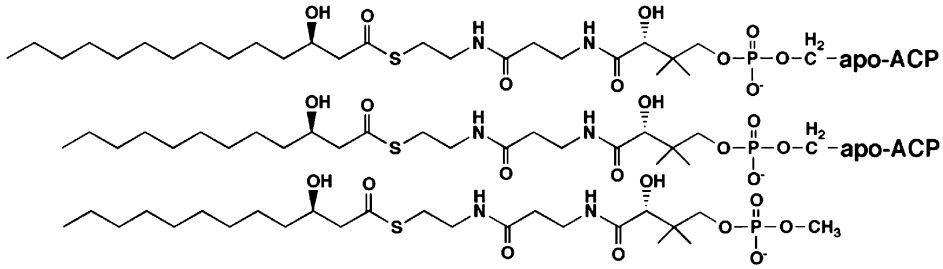

cosamine would not be expected to bind to the free form or the *R*-3-OHC$_{14}$-ACP-bound form of LpxD. Although the possibility that UDP-2,3-diacylglucosamine has some affinity for the free form of LpxD cannot be completely excluded, the data clearly show that UDP-2-*N*-(*R*-3-OHC$_{14}$)-GlcN is not a competitive inhibitor with respect to either substrate.

Inhibition of EcLpxD by (R)-3-Hydroxylauroyl-methylphosphopantetheine. (*R*)-3-Hydroxylauroyl-methylphosphopantetheine was synthesized (Table 2) because it represents a well-defined substructure of *R*-3-OHC$_{14}$-ACP. The phosphopantetheine moiety is covalently attached to Ser-36 of ACP. We found that (*R*)-3-hydroxylauroyl-methylphosphopantetheine is a very slow substrate for LpxD (Table 2). The specific activity, measured with either 10 μM (Table 2) or 1 mM (not shown) (*R*)-3-hydroxylauroyl-methylphosphopantetheine as the acyl donor, is >100-fold lower than with 10 μM *R*-3-OHC$_{14}$-ACP. The slow reactivity of (*R*)-3-hydroxylauroyl-methylphosphopantetheine as a substrate does not interfere with its use for the analysis of inhibition kinetics.

Surprisingly, (*R*)-3-hydroxylauroyl-methylphosphopantetheine is not a competitive inhibitor with respect to *R*-3-OHC$_{14}$-ACP (Figure 4). Instead, it is a competitive inhibitor with respect to UDP-3-*O*-(*R*-3-OHC$_{14}$)-GlcN with an apparent K_{ic} of 390 $\pm$ 70 μM and an uncompetitive inhibitor with respect to *R*-3-OHC$_{14}$-ACP with an apparent K_{iu} of 690 $\pm$ 100 μM (Figure 4). When substrate concentrations are taken into account, these inhibition constants are converted to a K_{ic} of 298 $\pm$ 53 μM and a K_{iu} of 394 $\pm$ 62 μM based on the K_M values calculated from Figure 2. These patterns suggest that (*R*)-3-hydroxylauroyl-methylphosphopantetheine actually binds to the same form of the enzyme that the substrate UDP-3-*O*-(*R*-3-OHC$_{14}$)-GlcN does. (*R*)-3-Hydroxylauroyl-methylphosphopantetheine does contain an (*R*)-3-hydroxyacyl chain and phosphate group like UDP-3-*O*-(*R*-3-OHC$_{14}$)-GlcN, so perhaps these two compounds can bind to the same form of the enzyme because the acyl chain and the phosphate group provide most of the binding energy. K_{ic} [for UDP-3-*O*-(*R*-3-OHC$_{14}$)-GlcN] and K_{iu} (for *R*-3-OHC$_{14}$-ACP) are within error of each other, consistent with the idea that both inhibition constants arise from the same (*R*)-3-hydroxylauroyl-methylphosphopantetheine binding process on the *R*-3-OHC$_{14}$-ACP-bound form of LpxD (Scheme 1). The fact that (*R*)-3-hydroxylauroyl-methylphosphopantetheine does not predominately bind to the free form of LpxD further suggests that the phosphopantetheine moiety contributes relatively little to the binding. This in turn suggests that the phosphopantetheine moiety of *R*-3-OHC$_{14}$-ACP likewise contributes relatively little to the interaction between free LpxD and *R*-3-OHC$_{14}$-ACP.

According to Scheme 1, if (*R*)-3-hydroxylauroyl-methylphosphopantetheine is a competitive inhibitor with respect to UDP-3-*O*-(*R*-3-OHC$_{14}$)-GlcN, it should be an uncompetitive inhibitor with respect to *R*-3-OHC$_{14}$-ACP. This is clearly the case (Figure 4), indicating that the preferred form of LpxD with which (*R*)-3-hydroxylauroyl-methylphosphopantetheine interacts is the *R*-3-OHC$_{14}$-ACP-bound form. As noted above, however, (*R*)-3-hydroxylauroyl-methylphosphopantetheine can also function as a poor substrate in the absence of *R*-3-OHC$_{14}$-ACP, suggesting that (*R*)-3-hydroxylauroyl-methylphosphopantetheine does in fact have a low affinity for the free form of EcLpxD or, perhaps, that EcLpxD employs a different kinetic mechanism when (*R*)-3-hydroxylauroyl-methylphosphopantetheine is the acyl donor.

Direct Evaluation of Substrate Binding by EcLpxD. To provide further evidence for Scheme 1, constants for binding of each substrate to free EcLpxD were estimated using spin column separations (*27, 28*). In this procedure, the ligand is

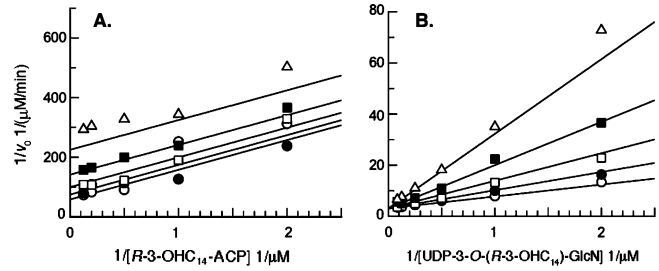

FIGURE 4: Inhibition of LpxD by (*R*)-3-hydroxylauroyl-methylphosphopantetheine. The plots display the Lineweaver−Burke representations of the initial velocities as a function of substrate concentration at increasing constant concentrations of the synthetic inhibitor (*R*)-3-hydroxylauroyl-methylphosphopantetheine. Substrate concentrations were varied as shown from 5-fold below to 5-fold above the K_M, while the other substrate was held at a constant concentration at approximately 2-fold above K_M. Nonlinear fits (displaying the lowest χ^2 values) were derived by least-squares fitting using GraFit.[2] (*R*)-3-Hydroxylauroyl-methylphosphopantetheine concentrations were held constant 0 (○), 0.2 (●), 0.5 (□), 1 (■), or 2 mM (△). (A) (*R*)-3-Hydroxylauroyl-methylphosphopantetheine is an uncompetitive inhibitor with respect to *R*-3-OHC$_{14}$-ACP. (B) (*R*)-3-Hydroxylauroyl-methylphosphopantetheine is a competitive inhibitor with respect to UDP-3-*O*-(*R*-3-OHC$_{14}$)-GlcN.

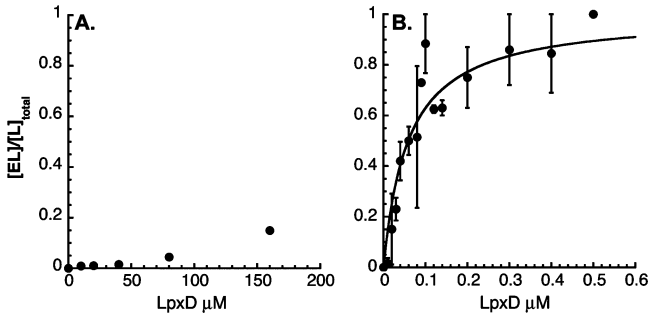

FIGURE 5: Direct measurement of substrate binding to free LpxD. (A) Pure LpxD (from 0 to 160 μM) was incubated with 24 nM [α-^{32}P]UDP-3-*O*-(*R*-3-OHC$_{14}$)-GlcN. (B) Pure LpxD (from 0 to 0.5 μM) was incubated with 5 nM *R*-3-OHC$_{14}$-ACP for 10 min. Free ligand was rapidly separated from bound ligand by centrifugation over a small Sephadex G-50 column (*28*). The fraction of ligand bound to enzyme (determined as described in Materials and Methods) is plotted as a function of total enzyme concentration. Equation 7 was fit to the data, and the K_d was estimated as >160 μM for UDP-3-*O*-(*R*-3-OHC$_{14}$)-GlcN and as 59 $\pm$ 8 nM for *R*-3-OHC$_{14}$-ACP.

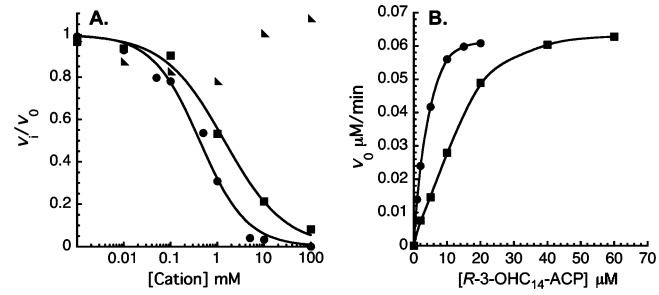

FIGURE 6: Effects of divalent cations on LpxD activity. (A) $CaCl_2$ (●), $MgCl_2$ (■), or NaCl (triangles) concentrations were varied from 0 to 100 mM, as indicated. To determine the IC_{50} for the divalent cations, eq 9 was fit to the data. (B) Ca^{2+} inhibition is overcome by increasing the *R*-3-OHC$_{14}$-ACP concentration. The initial velocities as a function of *R*-3-OHC$_{14}$-ACP concentration are shown with 0 (●) or 1 mM $CaCl_2$ (■) in the assay system, as indicated.

first incubated with excess enzyme and then unbound ligand is separated from bound ligand by rapid centrifugation over a small Sephadex G-50 column. Molecules with masses of >30 kDa (including the bound ligand) emerge in the run-through, whereas molecules with masses of <30 kDa are retained by the column.

The fraction of the [α-^{32}P]UDP-3-*O*-(*R*-3-OHC$_{14}$)-GlcN bound to excess EcLpxD ([EL]/[L]$_{total}$) was determined by liquid scintillation counting and evaluated using eq 6. Because the *R*-3-OHC$_{14}$-ACP ligand was not radiolabeled, the concentration of *R*-3-OHC$_{14}$-ACP bound to LpxD was determined indirectly by diluting a portion of the spin column run-through into an assay mixture that contained a 2-fold molar excess of [α-^{32}P]UDP-3-*O*-(*R*-3-OHC$_{14}$)-GlcN and $\geq$1 μM LpxD (single-turnover conditions). The amount of [α-^{32}P]UDP-2,3-diacylglucosamine product formed under these conditions was proportional to the concentration of *R*-3-OHC$_{14}$-ACP (i.e., that bound to LpxD) in the run-through. The resulting data were fit to eq 7 to determine the affinity of each substrate for the free form of LpxD. Figure 5 shows the binding isotherms for each substrate. [α-^{32}P]UDP-3-*O*-(*R*-3-OHC$_{14}$)-GlcN shows very little affinity for the free form of EcLpxD (K_d > 160 μM), whereas *R*-3-OHC$_{14}$-ACP shows a high affinity for free EcLpxD (K_d = 59 $\pm$ 8 nM). These findings independently support Scheme 1, in which *R*-3-OHC$_{14}$-ACP binds to the free form of LpxD and UDP-3-*O*-(*R*-3-OHC$_{14}$)-GlcN binds to the *R*-3-OHC$_{14}$-ACP-bound form.

Role of Acyl Carrier Protein in Binding. Table 2 shows the EcLpxD specific activities with the acyl donor substrates *R*-3-OHC$_{14}$-ACP, *R*/*S*-3-hydroxylauroyl-ACP, or (*R*)-3-hydroxylauroyl-methylphosphopantetheine (each at 10 μM of the *R*-form, assuming a 1:1 *R*:*S* ratio for the *R*/*S*-3-hydroxylauroyl-ACP) and UDP-3-*O*-(*R*-3-OHC$_{14}$)-GlcN (6 μM) as the acceptor. The assumption was also made that the *S*-form does not function as an acyl donor or inhibit the reaction. Removal of two carbons from the acyl chain reduces the LpxD specific activity by 10-fold. The additional loss of the acyl carrier protein portion of the substrate further reduces activity more than 100-fold (Table 2). The results show that the full-length 14-carbon acyl chain and the ACP protein itself are very important for efficient LpxD catalysis, presumably by providing optimal binding energy.

Divalent cation inhibition of EcLpxD activity provides independent evidence of the importance of the protein portion of *R*-3-OHC$_{14}$-ACP in LpxD catalysis. Divalent cations are known to bind key acidic side chains of *E. coli* ACP, which are often important for productive interaction of ACP with other proteins (*33*−*36*). Divalent cations such as Ca^{2+} and Mg^{2+} might inhibit LpxD activity by disrupting salt bridges between basic residues on EcLpxD and acidic residues on *R*-3-OHC$_{14}$-ACP. Various divalent and monovalent cations were therefore tested as inhibitors in the range of 0−100 mM with substrate concentrations held at 6 μM *R*-3-OHC$_{14}$-ACP and 4 μM UDP-3-*O*-(*R*-3-OHC$_{14}$)-GlcN. As shown in Figure 6A, Ca^{2+} inhibits LpxD with an IC_{50} of 0.42 $\pm$ 0.06 mM and Mg^{2+} with an IC_{50} of 1.41 $\pm$ 0.2 mM. Na^+ (Figure 6A) and K^+ ions (not shown) do not inhibit LpxD activity. These findings are consistent with reports that ACP has a high affinity for both $Ca^{2+}$and Mg^{2+} but only a weak affinity for Na^+ and K^+ (*37, 38*). Figure 6B shows that Ca^{2+} inhibition is overcome by the addition of excess *R*-3-OHC$_{14}$-ACP, consistent with the idea that Ca^{2+} is interacting with acidic sites on *R*-3-OHC$_{14}$-ACP, thereby rendering it less capable of interacting with LpxD.

To confirm that the protein portion of *R*-3-OHC$_{14}$-ACP is required for Ca^{2+} inhibition, we measured the specific activity of LpxD with either 10 μM *R*-3-OHC$_{14}$-ACP or 10 μM (*R*)-3-hydroxylauroyl-methylphosphopantetheine in the presence or absence of 10 mM Ca^{2+}. With *R*-3-OHC$_{14}$-ACP, the specific activity in the absence of Ca^{2+} was 7.14 $\times$ 10^3 nmol min^{-1} mg^{-1}, whereas in the presence of Ca^{2+}, it was 1.14 $\times$ 10^3 nmol min^{-1} mg^{-1}. In contrast, with (*R*)-3-hydroxylauroyl-methylphosphopantetheine as the acyl donor, the specific activity in the absence of Ca^{2+} was 3.0 nmol min^{-1} mg^{-1} versus 3.3 nmol min^{-1} mg^{-1} the presence of Ca^{2+}, consistent with the idea that Ca^{2+} interacts with the protein portion of *R*-3-OHC$_{14}$-ACP.

Approach to the Site-Directed Mutagenesis of EcLpxD. Residues for site-directed mutagenesis (Tables 3 and 4) were chosen by sequence alignment (*39, 40*) or were selected on the basis of the CtLpxD crystal structure (*14*). The CtLpxD residues and atoms listed in Table 3 are potentially close enough to the bound UDP-GlcNAc ligand ($\leq$3.3 Å) to engage in polar interactions (*14*). Table 4 shows the residues

Table 3: Differences in UDP-GlcNAc Binding between Chains A and B of CtLpxD Complex I versus CtLpxD Complex II

CtLpxD residue and heteroatom near UDP-GlcNAc	corresponding EcLpxD residue[a]	possible H-bond or polar partner on UDP-GlcNAc	distance[b] (Å) in Complex I	distance[b] (Å) in Complex II
		Chain A		
F190 O		GlcNAc O4	2.67[e]	8.14[e]
Y192 N		GlcNAc O6	3.15[e]	11.3[e]
H247 NE2[c]	H239	GlcNAc O3	3.07[e]	6.71[e]
H247 NE2	H239	GlcNAc O7[d]	5.01[e]	2.61[e]
H247 NE2	H239	GlcNAc N2	4.50	4.60
Q248 OE1	N240	ribose O3	3.03	2.92
Q248 NE2	N240	ribose O3	3.30	3.66
G265 O		GlcNAc O7[d]	2.35[e]	5.74[e]
S266 OG	S258	ribose O3	2.78	3.93
H284 NE2	H276	PO α1	3.11	2.70
H284 NE2	H276	PO β2	3.34	2.53
H284 NE2	H276	GlcNAc O7[d]	3.21[e]	5.42[e]
H284 NE2	H276	GlcNAc N2	3.19[e]	4.69[e]
		Chain B		
E32 OE2		ribose O3	3.40	2.62
I33 N		uracil O2	2.82	2.80
E34 OE1	Q32	ribose O2	4.50	3.01
F43 O	F41	uracil N3	2.93	2.68
D45 N		uracil O4	2.82	2.78
N46 N	N44	uracil O4	3.50	3.26
N46 ND2	N44	GlcNAc O6	8.77[e]	3.09[e]
N46 ND2	N44	PO β1	3.84	3.23
Y49 OH	Y47	PO β2	3.08	2.40

[a] Residues subjected to site-directed mutagenesis in EcLpxD; see Table 4. [b] Distance measurements were made using PyMol (DeLano Scientific, San Carlos, CA) on PDB entry 2iu8 for Complex I and PDB entry 2iu9 for Complex II (*14*). [c] H247 distances are based on the proper rotamer predicted by MolProbity (*52, 53*). [d] O7 is the carbonyl oxygen of the acetyl moiety. [e] Distance discrepancies of >1.50 Å in the positioning of UDP-GlcNAc in Complex I vs Complex II.

Table 4: Steady-State Kinetic Parameters for Selected EcLpxD Mutants

EcLpxD protein	k_{cat} (s^{-1})	$K_{M,UDP\text{-}3\text{-}O\text{-}(R\text{-}3\text{-}OHC_{14})\text{-}GlcN}$ (μM)	$K_{M,R\text{-}3\text{-}hydroxymyristoyl\text{-}ACP}$ (μM)
wild type	23 ± 1	2.5 ± 0.3	3.2 ± 0.8
group I			
F41A	4.1 ± 0.9	73 ± 30	3.5 ± 0.5
Y47A	18 ± 3	7.8 ± 3	5 ± 1
H239A	0.032 ± 0.001	0.84 ± 0.1	3.4 ± 1
H276A	0.73 ± 0.3	6.3 ± 0.9	1.7 ± 0.4
group II			
D232A	1.9 ± 0.1	67 ± 10	47 ± 7
N233A	1.4 ± 0.1	28 ± 7	13 ± 4
Q236A	12 ± 1	4.2 ± 0.9	13 ± 3
group III			
K46A	17 ± 1	7.1 ± 1	12 ± 5
K194A	5.7 ± 0.2	5.6 ± 0.5	3.8 ± 0.9
R293A	8.9 ± 0.7	3.6 ± 1.0	74 ± 0.3

that were subjected to mutagenesis in EcLpxD. Group I residues (Table 4) correspond to those near the UDP-GlcNAc binding site in CtLpxD Complexes I and II (Table 3) (*14*). Group II residues (Table 4) correspond to those near the carboxyl group of the bound palmitic acid seen in CtLpxD Complexes I and II (*14*). Group III residues are other conserved basic side chains (*14*) that might be involved in acyl-ACP binding.

Two Modes of UDP-GlcNAc Binding in CtLpxD. Given the superior 2.2 Å resolution of Complex I, which contains a single bound UDP-GlcNAc between chains A and B (PDB entry 2iu8) (*14*), and the good electron density of the UDP-GlcNAc ligand situated between chains A and B in 3.1 Å Complex II (PDB entry 2iu9) (*14*), we focused on these two sites (Table 3). All protein heteroatoms within 3.3 Å of plausible H-bonding or polar partners on the UDP-GlcNAc in Complex I or II (or both) were evaluated (Table 3).

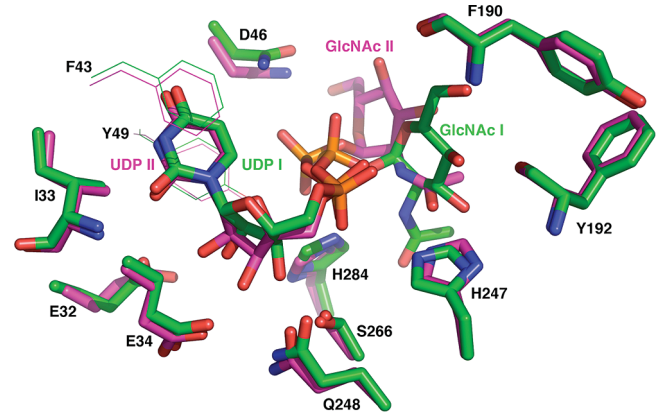

FIGURE 7: Overlay of the UDP-GlcNAc ligand located between CtLpxD chains A and B in Complex I vs Complex II. The UDP-GlcNAc carbons of Complex I are colored green, whereas those of Complex II are colored magenta (*14*). The positions of the CtLpxD side chains (green sticks for Complex I and magenta sticks for Complex II) are very similar in both complexes (*14*), but the GlcNAc moiety of the bound UDP-GlcNAc is displaced by more than 90°, accounting for the dramatic differences in some of the interatomic distances listed in Table 3. The side chains of the two aromatic residues that flank the uracil moiety (*14*) are shown as lines for clarity.

The distances between key atoms of the UDP moiety of the bound UDP-GlcNAc and various CtLpxD side chains are quite similar in Complexes I and II (Table 3, numbers without a footnote). However, there are large differences between these two complexes in the distances between key side chains of CtLpxD and the heteroatoms of the GlcNAc moiety. Discrepancies greater than 1.5 Å are denoted with footnote e (Table 3). These anomalies are easily explained when the UDP-GlcNAc ligand of Complex I is overlaid onto its counterpart in Complex II (Figure 7, sticks). The UDP moieties of the two complexes display similar conformations, accounting for the relatively consistent interatomic distances (Table 3). However, the GlcNAc group is flipped in Complex I versus Complex II (Figure 7, sticks). The positions of the surrounding LpxD side chains are very similar in both complexes (Figure 7, magenta sticks and lines vs green sticks and lines). Why the GlcNAc moiety is oriented differently in Complexes I and II is uncertain and was not discussed by Buetow et al. (*14*).

Site-Directed Mutagenesis of EcLpxD Group I Residues. As shown in Table 4, the conserved EcLpxD residue H239 is critically important for enzymatic activity. It likely functions as the general base to activate the amine group of the acceptor substrate during catalysis (Scheme 2). When H239 is mutated to alanine, the k_{cat} of EcLpxD is reduced 1000-fold with very little effect on the K_M of either substrate (Table 4). Conserved in all LpxD sequences, H239 of EcLpxD (equivalent to H247 of CtLpxD) (*14*) also aligns with H125 in *E. coli* LpxA (*15, 17*); the Nε2 atom of the latter is the general base in LpxA, being situated within H-bonding distance of the GlcNAc 3-OH group in the LpxA structure and functioning to activate it for attack on the thioester carbonyl moiety of acyl-ACP (*16, 17*). Our sug-

Scheme 2: Possible Roles of H239 and G257 in the Catalytic Mechanism of *E. coli* LpxD[a]

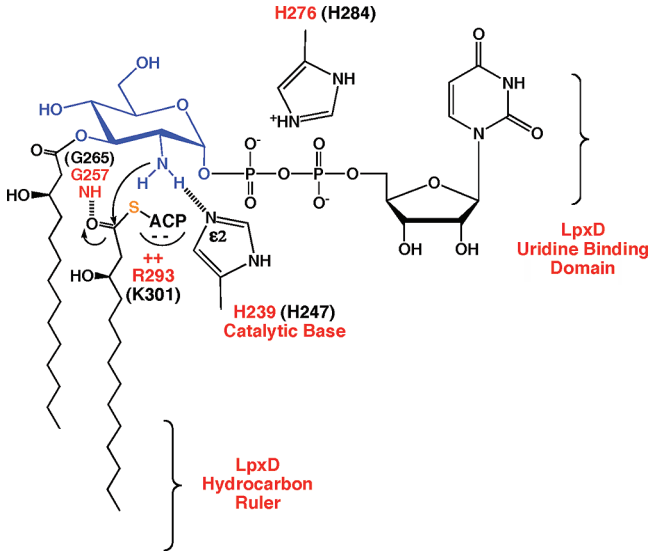

[a] After the ternary complex is formed, the Nε2 atom of H239 activates the amine group of UDP-3-*O*-(*R*-3-OHC_{14})-GlcN (blue), which then attacks the carbonyl moiety of *R*-3-OHC_{14}-ACP. R293 of EcLpxD may contribute to binding of the acyl-ACP donor substrate by providing ionic interactions. The tetrahedral intermediate is presumably stabilized by the oxyanion hole at G257 of EcLpxD. H276 functions mainly to bind the diphosphate moiety of the acceptor substrate. EcLpxD residue numbers are in red, and corresponding CtLpxD residue numbers are in black.

gestion that H239 of EcLpxD is the catalytic base is, however, inconsistent with the CtLpxD structure (Table 3) (*14*). Nε2 of H247 of CtLpxD is 4.5 and 4.6 Å from the N2 atom of the GlcNAc moiety in Complexes I and II, respectively (Table 3), too far to activate the N2 atom of the substrate (*14*). Buetow et al. (Figure 1 in ref *14*) therefore propose that H247 of CtLpxD (corresponding to H239 of EcLpxD) and H284 of CtLpxD (corresponding to H276 of EcLpxD) stabilize the oxyanion intermediate.

On the basis of our analysis, H276 of EcLpxD (H284 of CtLpxD) may function in acceptor substrate binding but not in catalysis. We see a modest (30-fold) reduction in k_{cat} in the H276A mutant (Table 4), suggesting that H276 is not likely to be involved in stabilization of the oxyanion intermediate as proposed by Buetow et al. (*14*). In both Complexes I and II, however, H284 of CtLpxD is well positioned to participate in binding the diphosphate moiety of the acceptor substrate (Table 3 and Figure 7) (*14*).

In the CtLpxD structure, several additional residues were implicated in binding UDP-GlcNAc (*14*). In Complexes I and II, F43 and Y49 create π-stacking interactions with the uracil base, and the backbone carbonyl oxygen of F43 provides an important H-bond acceptor (Table 3). The corresponding EcLpxD F41A variant displays a 30-fold increase in $K_{M,UDP\text{-}3\text{-}O\text{-}(R\text{-}3\text{-}OHC_{14})\text{-}GlcN}$ and a 5-fold decrease in k_{cat}, consistent with its position in the crystal structure (*14*). However, the EcLpxD substitution Y47A (Table 4) has an only small effect on $K_{M,UDP\text{-}3\text{-}O\text{-}(R\text{-}3\text{-}OHC_{14})\text{-}GlcN}$ (a 3-fold increase) with little effect on k_{cat} or $K_{M,R\text{-}3\text{-}OHC_{14}\text{-}ACP}$.

E34 and N46 in CtLpxD Complex I are proposed to hydrogen bond the 2′-hydroxyl group of the ribose ring and the β-phosphate group, respectively, of UDP-GlcNAc (Table 3), whereas Q248 hydrogen bonds to the ribose 3′-hydroxyl group (*14*). In our analysis of EcLpxD, the corresponding residues (Table 3) contribute little to the binding of the native EcLpxD substrates. The corresponding EcLpxD substitutions, Q32A, N44A, and N240A, caused a <2-fold reduction in specific activity, when assayed at substrate concentrations 2-fold above the K_M with the purified proteins (data not shown).

Site-Directed Mutagenesis of EcLpxD Group II Residues. The CtLpxD structure revealed the presence of an extraneous fatty acid in each subunit (*14*), situated in a hydrophobic groove within the Lβ*H* domains of the protein. Aliphatic residues line the walls of this groove. In addition, three polar CtLpxD residues, D240, N241, and Q244 (corresponding to D232, N233, and Q236 in EcLpxD, respectively), are close to the carboxylate moiety of the bound fatty acid. The EcLpxD mutations D232A and N233A caused a 10-fold reduction in k_{cat} and a striking increase in the K_M for both substrates, suggesting they are somehow involved in binding of the physiological substrates, whereas the Q236A mutation had little effect on activity (Table 4).

Site Directed Mutagenesis of EcLpxD Group III Residues. As noted above (Figure 6 and Table 2), acidic side chains on *R*-3-OHC_{14}-ACP may be important for its binding to LpxD. Consequently, LpxD may contain cognate basic residues that interact with *R*-3-OHC_{14}-ACP. The CtLpxD structure reveals a basic cleft near the active site around the highly conserved K48 residue (K46 in EcLpxD) (*14*). As shown in Table 4, however, the K46A substitution in EcLpxD caused an only 3-fold increase in $K_{M,R\text{-}3\text{-}OHC_{14}\text{-}ACP}$ and had no effect on k_{cat}. Mutation of another basic residue close to the active site, K194 (H202 in CtLpxD), to alanine likewise had little effect on activity (Table 4).

Although it was not considered in the analysis of the crystal structure (*14*), we noticed another conserved basic residue in the general vicinity of the active site, R293, which has a dramatic effect on catalysis when mutated to alanine (Table 4). The $K_{M,R\text{-}3\text{-}OHC_{14}\text{-}ACP}$ for R293A increases 23-fold compared to that of the wild type with little effect on k_{cat} (Table 4), suggesting a role for R293 in *R*-3-OHC_{14}-ACP binding (Scheme 2).

DISCUSSION

LpxD catalyzes the third step of lipid A biosynthesis in *E. coli*, the *R*-3-OHC_{14}-ACP-dependent N-acylation of UDP-3-*O*-(*R*-3-OHC_{14})-GlcN (Figure 1A) (*9, 41*). A crystal structure of *C. trachomatis* LpxD has recently appeared (*14*), demonstrating that LpxD resembles LpxA (*10, 17, 42, 43*) in its homotrimeric architecture and β-helical fold (Figure 1B,C). However, little is known about the chemical mechanism of LpxD or how it recognizes its physiological substrates (panel A of Figure 1A vs panel C). Because lipid A is required for the growth of most Gram-negative bacteria (*3*), LpxD inhibitors should be useful as antibiotics, but to date, no inhibitors with antibacterial activity have been identified. A possible advantage of LpxD inhibitors over the many available LpxC inhibitors (*1, 3, 4*) might be the intracellular accumulation of the intermediate UDP-3-*O*-(*R*-3-OHC_{14})-GlcN (Figure 1A), a detergent-like molecule that could enhance cell killing.

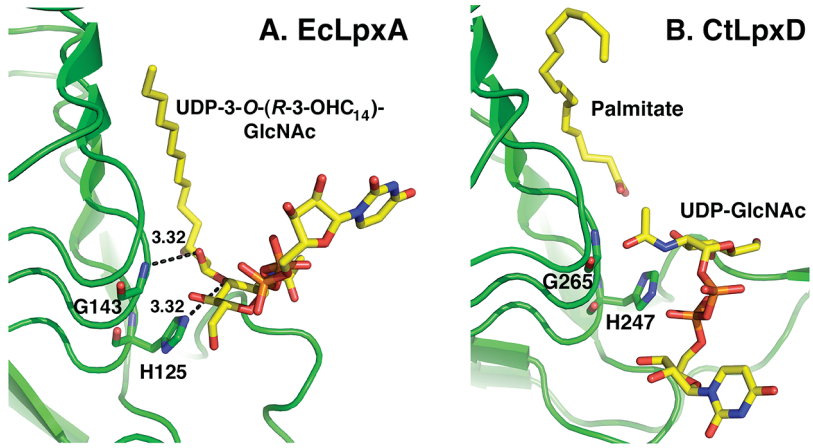

FIGURE 8: Comparison of the catalytic base and oxyanion hole in LpxA and LpxD. (A) H125 of EcLpxA is positioned to hydrogen bond to the O3 atom of the GlcNAc moiety, whereas the backbone N atom of G143 (one turn of the β-helix distal to H125) is positioned to stabilize the putative oxyanion intermediate, given its proximity to the ester carbonyl in the bound UDP-3-*O*-(*R*-3-hydroxymyristoyl)-GlcNAc product seen in the crystal structure of the EcLpxA−UDP-3-*O*-(*R*-3-hydroxymyristoyl)-GlcNAc complex (*17*). Dashed lines represent the interatomic distances in angstroms. (B) The conserved H247 residue of CtLpxD, which aligns with H125 of LpxA in sequence comparisons, is proposed to hydrogen bond to the N2 GlcN atom of the physiological LpxD substrate (see Scheme 2). Shown here is the positioning of the conserved CtLpxD H247 side chain relative to the N atom of the bound nonphysiological ligand, UDP-GlcNAc, as seen in Complex I (*14*). The Nε2 atom of H247 is too far removed to engage in a hydrogen bond with the N2 atom of the GlcNAc moiety (4.5 Å). However, given the uncertainties in the GlcNAc conformation (Figure 7), the possible differences in the binding of the physiological LpxD acceptor substrate vs UDP-GlcNAc, and the profound loss of activity caused by the H239A mutation in EcLpxD (Table 4), H247 is nevertheless proposed to be the general base. CtLpxD also contains the conserved G265 residue (one turn of the β-helix distal to H247), the backbone NH moiety of which could function as the oxyanion hole, exactly like that of G143 in EcLpxA. The color scheme is the same as in Figure 1C.

As a prelude to the search for antibacterial LpxD inhibitors, EcLpxD has been subjected to kinetic studies and site-directed mutagenesis (*9*). Our kinetic data suggest a predominantly compulsory-ordered mechanism for EcLpxD in which *R*-3-OHC_{14}-ACP binds prior to UDP-3-*O*-(*R*-3-OHC_{14})-GlcN and UDP-2,3-diacylglucosamine dissociates prior to ACP (Scheme 1). The following results support this conclusion. (a) ACP is a competitive inhibitor with respect to *R*-3-OHC_{14}-ACP and a noncompetitive inhibitor with respect to UDP-3-*O*-(*R*-3-OHC_{14})-GlcN (Figure 3). (b) UDP-2-*N*-(*R*-3-OHC_{14})-GlcN is a noncompetitive inhibitor with respect to both substrates (Figure 3). (c) (*R*)-3-Hydroxylauroylmethylphosphopantetheine is an uncompetitive inhibitor with respect to *R*-3-OHC_{14}-ACP and a competitive inhibitor with respect to UDP-3-*O*-(*R*-3-OHC_{14})-GlcN (Figure 4). (d) *R*-3-OHC_{14}-ACP displays a high affinity for free LpxD, whereas UDP-3-*O*-(*R*-3-OHC_{14})-GlcN does not (Figure 5). Our data are consistent with results obtained for related enzymes, such as serine acetyltransferase, galactoside acetyltransferase, and *sn*-glycerol-3-phosphate acyltransferase, which likewise proceed through analogous ordered mechanisms (*13*).

On the basis of multiple-sequence alignments, H239 of EcLpxD is equivalent to H247 of CtLpxD, and both align with H125 of LpxA (Figure 8A), the catalytic base as determined by structural studies and mutagenesis of LpxA (*15*−*17*). As shown by the 1000-fold reduction in k_{cat} of the H239A mutant (Table 4), H239 of EcLpxD is now directly implicated as the catalytic base. However, the corresponding H247 residue in the CtLpxD structure (*14*) is not properly positioned either in Complex I or in Complex II (Table 3 and Figure 7) to hydrogen bond to the N2 atom of the GlcN moiety of UDP-GlcNAc, nor is it likely to stabilize the oxyanion intermediate (see below), as suggested by Buetow et al. (*14*).

Our data reveal an only 30-fold reduction in the k_{cat} of the EcLpxD H276A mutant (Table 4), which argues against the direct participation of this residue (or of CtLpxD H284) in any aspect of catalysis, such as the proposed stabilization of the oxyanion intermediate (*14*). The alternative that CtLpxD H284 is important for substrate binding is, however, compatible with its positioning relative to the diphosphate group of UDP-GlcNAc, which is similar in both Complexes I and II (Figure 7) (*14*). The reasons for the dramatic differences in the orientations of the GlcNAc moieties in the two complexes (Figure 7) are not known (*14*).

As noted, Buetow et al. suggested that both H247 and H284 of CtLpxD could stabilize the oxyanion intermediate formed during LpxD catalysis (Figure 1 in ref *14*). This possibility is consistent with the structure of Complex II for H247 or with the structure of Complex I for H284 (Table 3), but not with both structures for both histidines, given the differences in the positioning of the GlcNAc residue in the two complexes (Table 3 and Figure 7) (*14*). Furthermore, because most oxyanion "holes" in serine proteases (*44*), protein *N*-myristoyltransferases (*45*), and lipases (*46*) feature backbone NH groups, we favor the alternative mechanistic scenario, shown in Scheme 2 and Figure 8. As noted above, we propose that EcH239 (CtH247) is the catalytic base whereas EcH276 (CtH284) is involved in substrate binding (Table 4). We suggest that the backbone NH group of the absolutely conserved EcLpxD G257 residue (G265 in CtLpxD), located one turn of the β-helix distal to H239 of EcLpxD (H247 of CtLpxD), stabilizes the oxyanion intermediate (Scheme 2 and Figure 8B). The equivalent residue (G143 in *E. coli* LpxA) is likewise present in all LpxA sequences, and its function as the oxyanion hole can be inferred directly from structural studies of the LpxA−3-*O*-(*R*-3-hydroxymyristoyl)-GlcNAc product complex (Figure 8A) in which the G143 backbone NH group of LpxA is appropriately positioned (*17*).

Previous studies have suggested that the catalytic histidine residues of the acyltransferases of the LβH family may be

hydrogen bonded to (and/or be oriented by) an adjacent negatively charged atom (*13*). The side chain of D126 serves this purpose for H125 in *E. coli* LpxA (*15, 17*); a backbone threonine carbonyl group plays this role in the *Pseudomonas aeuroginosa* xenobiotic acetyltransferase (*12*), and an aspartate side chain is utilized in *E. coli* serine acetyl transferase (*47*). Given the conservation of D126 in most LpxA sequences, the homologous EcLpxD N240 residue seemed to be a possible candidate for interaction with EcLpxD H239. However, the N240A mutation had no effect on EcLpxD activity (data not shown). Furthermore, Q248 (the residue corresponding to N240 in CtLpxD) is too far removed (>4.5 Å) to interact with H247 in CtLpxD (*14*), and on the basis of the structure, the Q248 side chain is instead hydrogen bonded to the ribose 3-OH group of UDP-GlcNAc (*14*) (Table 3).

From the *C. trachomatis* LpxD structure determined with bound UDP-GlcNAc (*14*), several additional residues were deemed to be important in substrate binding. Unlike the GlcNAc moieties, the UDP groups of the bound UDP-GlcNAc ligands were quite similar in both Complexes I and II (Figure 7). F43 and Y49 (F41 and Y47 in EcLpxD, respectively) form π-stacking interactions with uracil moiety as part of a novel uridine-binding domain (*14*). Our mutagenesis data support the idea that F41 (F43 in CtLpxD) indeed plays an important role in nucleotide binding (Table 4). Two other side chains in CtLpxD, E34 and N46, may be involved in hydrogen bonding to the 2-OH group of the ribose ring and the PO β1 atom, respectively, albeit only in Complex II (Table 3). The corresponding *E. coli* mutants (Q32A and N44A) have a <2-fold effect on activity, suggesting that these residues contribute little to the binding of the nucleotide substrate. Alternatively, *E. coli* and *C. trachomatis* LpxD may engage their ligands differently, or the physiological LpxD substrates may interact with CtLpxD in a manner different from that of UDP-GlcNAc and free fatty acids. In future structural studies of LpxD, it will be desirable to use physiological substrates as bound ligands (Figure 1A) to make stronger mechanistic conclusions.

It is unclear whether the free fatty acids observed in the CtLpxD crystal structure (Figure 1C) occupy the acyl chain binding site of the acyl-ACP donor substrate or of the UDP-3-*O*-(acyl)-glucosamine acceptor. In this regard, it is worth noting that EcLpxD and CtLpxD must contain hydrocarbon rulers to ensure the incorporation of the proper N-linked hydroxyacyl chain. In the case of EcLpxD, this ruler is highly selective for 14 carbons (*9*), whereas CtLpxD presumably prefers 20 carbons (*14*). However, in *E. coli* LpxD, there is much less acyl chain selectivity with regard to the acceptor substrate. If the *E. coli lpxA* gene is inactivated by mutation and replaced with the *Pseudomonas lpxA* gene, which encodes a C10-specific acyltransferase (*48, 49*), the cells are viable, but a hybrid lipid A structure is synthesized in which the 3-O-linked hydroxyacyl chains are mostly hydroxydecanoate. However, the N-linked hydroxyacyl chains are still predominantly hydroxymyristate, as in wild-type cells (*48*). This result demonstrates that LpxD efficiently utilizes an acceptor substrate containing a C10 hydroxyacyl chain in living cells. As noted by Kelly et al. (*9*), however, UDP-GlcN (lacking an acyl chain) is a very poor substrate for LpxD, indicating the presence on LpxD of an important hydrophobic pocket for the 3-O-linked acyl chain on the acceptor substrate. This pocket appears to be less selective than the acyl chain binding pocket of the acyl-ACP donor substrate.

ACP is small acidic protein, present in a dynamic equilibrium of two or more conformers (*50*). This equilibrium is governed in part by the concentration of divalent cations, which bind to acidic residues on ACP (*37, 38*). Divalent calcium and magnesium cations have high affinities for these sites, with an average K_d of 80 μM (*38*). These divalent cation-binding sites lie along helix II of ACP. Various binding, mutagenesis, and docking studies have implicated helix II of ACP as the "recognition helix" that facilitates interaction with various enzymes (*33*−*36*). The recognition helix contains two acidic subsites: site A, composed of residues E30, D35, D38, and E41, and site B, composed of residues E47, D51, E53, and D56 (*51*).

Three observations suggest that the divalent cation-binding sites on ACP are important for interaction with LpxD. First, divalent cations inhibit LpxD activity (Figure 6A). Furthermore, divalent cation inhibition is overcome by increasing the concentration of *R*-3-OHC$_{14}$-ACP (Figure 6B). Finally, removal of the protein portion of ACP [for instance, when (*R*)-3-hydroxylauroyl-methylphosphopantetheine is used as the acyl donor] reduces activity more than 100-fold but eliminates divalent cation inhibition (Table 2).

Although we suspect that the acidic sites on ACP interact with LpxD, we still do not understand how LpxD recognizes ACP. The CtLpxD structure revealed a conserved basic residue at K48 (K46 in EcLpxD) that might be part of a basic cleft for ACP binding (*14*). However, the corresponding K46A mutant of EcLpxD displays an only 3-fold increase in the $K_{M,R\text{-}3\text{-}OHC_{14}\text{-}ACP}$ with no effect on k_{cat}. This finding suggests that K46 of EcLpxD or K48 of CtLpxD plays at best a minor role in the interaction of LpxD with ACP. In contrast, we have found that R293 (K301 in CtLpxD), a conserved basic residue that was not considered in the structural analysis (*14*), plays a significant role in the binding of *R*-3-OHC$_{14}$-ACP (Table 4 and Scheme 2). Given the distance of K301 from the active site of CtLpxD (approximately 18 Å), it may be that R293 of EcLpxD or K301 of CtLpxD interacts with the site A residues on ACP. Structural studies of LpxD−acyl-ACP complexes will be required to address these issues.

ACKNOWLEDGMENT

We thank Dr. Dale Christensen for construction of pDC015-1 and Dr. Ziquiang Guan for help with the mass spectrometry of LpxD.

SUPPORTING INFORMATION AVAILABLE

Methods for the preparation of substrates and reagents, including *R*-3-OHC$_{14}$-ACP, *R*/*S*-3-hydroxylauroyl-ACP, [α-^{32}P]-UDP-GlcNAc, and [α-^{32}P]UDP-3-*O*-(*R*-3-OHC$_{14}$)-GlcN, and purification of untagged EcLpxD and His$_6$-EcLpxD, including criteria used to assess purity. This material is available free of charge via the Internet at http://pubs.acs.org.

REFERENCES

1. Raetz, C. R. H., and Whitfield, C. (2002) Lipopolysaccharide endotoxins. *Annu. Rev. Biochem. 71*, 635–700.

2. Nikaido, H. (2003) Molecular basis of bacterial outer membrane permeability revisited. *Microbiol. Mol. Biol. Rev. 67*, 593–656.
3. Raetz, C. R. H., Reynolds, C. M., Trent, M. S., and Bishop, R. E. (2007) Lipid A modification systems in Gram-negative bacteria. *Annu. Rev. Biochem. 76*, 295–329.
4. McClerren, A. L., Endsley, S., Bowman, J. L., Andersen, N. H., Guan, Z., Rudolph, J., and Raetz, C. R. H. (2005) A slow, tight-binding inhibitor of the zinc-dependent deacetylase LpxC of lipid A biosynthesis with antibiotic activity comparable to ciprofloxacin. *Biochemistry 44*, 16574–16583.
5. Gay, N. J., and Gangloff, M. (2007) Structure and function of toll receptors and their ligands. *Annu. Rev. Biochem. 76*, 141–165.
6. Kim, H. M., Park, B. S., Kim, J. I., Kim, S. E., Lee, J., Oh, S. C., Enkhbayar, P., Matsushima, N., Lee, H., Yoo, O. J., and Lee, J. O. (2007) Crystal structure of the TLR4-MD-2 complex with bound endotoxin antagonist Eritoran. *Cell 130*, 906–917.
7. Lynn, M., Rossignol, D. P., Wheeler, J. L., Kao, R. J., Perdomo, C. A., Noveck, R., Vargas, R., D'Angelo, T., Gotzkowsky, S., and McMahon, F. G. (2003) Blocking of responses to endotoxin by E5564 in healthy volunteers with experimental endotoxemia. *J. Infect. Dis. 187*, 631–639.
8. Russell, J. A. (2006) Management of sepsis. *N. Engl. J. Med. 355*, 1699–1713.
9. Kelly, T. M., Stachula, S. A., Raetz, C. R. H., and Anderson, M. S. (1993) The *firA* gene of *Escherichia coli* encodes UDP-3-*O*-(*R*-3-hydroxymyristoyl)-glucosamine *N*-acyltransferase: The third step of endotoxin biosynthesis. *J. Biol. Chem. 268*, 19866–19874.
10. Raetz, C. R. H., and Roderick, S. L. (1995) A left-handed parallel β helix in the structure of UDP-*N*-acetylglucosamine acyltransferase. *Science 270*, 997–1000.
11. Wang, X. G., Olsen, L. R., and Roderick, S. L. (2002) Structure of the *lac* operon galactoside acetyltransferase. *Structure 10*, 581–588.
12. Beaman, T. W., Sugantino, M., and Roderick, S. L. (1998) Structure of the hexapeptide xenobiotic acetyltransferase from *Pseudomonas aeruginosa*. *Biochemistry 37*, 6689–6696.
13. Vetting, M. W., de Carvalho, L. P. S., Yu, M., Hegde, S. S., Magnet, S., Roderick, S. L., and Blanchard, J. S. (2005) Structure and functions of the GNAT superfamily of acetyltransferases. *Arch. Biochem. Biophys. 433*, 212–226.
14. Buetow, L., Smith, T. K., Dawson, A., Fyffe, S., and Hunter, W. N. (2007) Structure and reactivity of LpxD, the *N*-acyltransferase of lipid A biosynthesis. *Proc. Natl. Acad. Sci. U.S.A. 104*, 4321–4326.
15. Wyckoff, T. J., and Raetz, C. R. H. (1999) The active site of *Escherichia coli* UDP-*N*-acetylglucosamine acyltransferase. Chemical modification and site-directed mutagenesis. *J. Biol. Chem. 274*, 27047–27055.
16. Ulaganathan, V., Buetow, L., and Hunter, W. N. (2007) Nucleotide Substrate Recognition by UDP-N-acetylglucosamine Acyltransferase (LpxA) in the First Step of Lipid A Biosynthesis. *J. Mol. Biol. 369*, 305–312.
17. Williams, A. H., and Raetz, C. R. H. (2007) Structural basis for the acyl chain selectivity and mechanism of UDP-N-acetylglucosamine acyltransferase. *Proc. Natl. Acad. Sci. U.S.A. 104*, 13543–13550.
18. Johnson, C. M., Huang, B., Roderick, S. L., and Cook, P. F. (2004) Chemical mechanism of the serine acetyltransferase from *Haemophilus influenzae*. *Biochemistry 43*, 15534–15539.
19. Roderick, S. L. (2005) The lac operon galactoside acetyltransferase. *C. R. Biol. 328*, 568–575.
20. Lo Leggio, L., Dal Degan, F., Poulsen, P., Andersen, S. M., and Larsen, S. (2003) The structure and specificity of *Escherichia coli* maltose acetyltransferase give new insight into the LacA family of acyltransferases. *Biochemistry 42*, 5225–5235.
21. Anderson, M. S., Bull, H. S., Galloway, S. M., Kelly, T. M., Mohan, S., Radika, K., and Raetz, C. R. H. (1993) UDP-*N*-acetylglucosamine acyltransferase of *Escherichia coli*: The first step of endotoxin biosynthesis is thermodynamically unfavorable. *J. Biol. Chem. 268*, 19858–19865.
22. Hayman, M. W., Fawcett, T., and Slabas, A. R. (2002) Kinetic mechanism and order of substrate binding for sn-glycerol-3-phosphate acyltransferase from squash (*Cucurbita moschata*). *FEBS Lett. 514*, 281–284.
23. Jackman, J. E., Raetz, C. R. H., and Fierke, C. A. (1999) UDP-3-O-(R-3-hydroxymyristoyl)-N-acetylglucosamine deacetylase of *Escherichia coli* is a zinc metalloenzyme. *Biochemistry 38*, 1902–1911.
24. Sugar, D., and Foxx, J. J. (1952) Spectrophotometric studies op nucleic acid derivatives and related compounds as a function of pH: I. Pyrimidines. *Biochim. Biophys. Acta 9*, 199–218.
25. Miller, J. R. (1972) *Experiments in Molecular Genetics*, Cold Spring Harbor Laboratory Press, Plainview, NY.
26. Smith, P. K., Krohn, R. I., Hermanson, G. T., Mallia, A. K., Gartner, F. H., Provenzano, M. D., Fujimoto, E. K., Goeke, N. M., Olson, B. J., and Klenk, D. C. (1985) Measurement of protein using bicinchoninic acid. *Anal. Biochem. 150*, 76–85.
27. Sambrook, J., Fritsch, E. F., and Maniatis, T. (1989) *Molecular Cloning: A Laboratory Manual*, 2nd ed., Cold Spring Harbor Laboratory Press, Plainview, NY.
28. Penefsky, H. S. (1979) A centrifuged-column procedure for the measurement of ligand binding by beef heart F1. *Methods Enzymol. 56*, 527–530.
29. Beebe, J. A., and Fierke, C. A. (1994) A kinetic mechanism for cleavage of precursor $tRNA^{Asp}$ catalyzed by the RNA component of *Bacillus subtilis* ribonuclease P. *Biochemistry 33*, 10294–10304.
30. Das, A. K., and Hajra, A. K. (1992) Critical micellar concentrations of palmitoyl dehydroxyacetone phosphate and 1-palmitoyl-rac-glycerol 3-phosphate. *J. Biol. Chem. 267*, 9731.
31. Cleland, W. W. (1977) *Adv. Enzymol. 45*, 273–387.
32. Radika, K., and Raetz, C. R. H. (1988) Purification and properties of lipid A disaccharide synthase of *Escherichia coli*. *J. Biol. Chem. 263*, 14859–14867.
33. Worsham, L. M., Earls, L., Jolly, C., Langston, K. G., Trent, M. S., and Ernst-Fonberg, M. L. (2003) Amino acid residues of *Escherichia coli* acyl carrier protein involved in heterologous protein interactions. *Biochemistry 42*, 167–176.
34. Zhang, Y. M., Marrakchi, H., White, S. W., and Rock, C. O. (2003) The application of computational methods to explore the diversity and structure of bacterial fatty acid synthase. *J. Lipid Res. 44*, 1–10.
35. Zhang, Y. M., Rao, M. S., Heath, R. J., Price, A. C., Olson, A. J., Rock, C. O., and White, S. W. (2001) Identification and analysis of the acyl carrier protein (ACP) docking site on β-ketoacyl-ACP synthase III. *J. Biol. Chem. 276*, 8231–8238.
36. Zhang, Y. M., Wu, B., Zheng, J., and Rock, C. O. (2003) Key residues responsible for acyl carrier protein and β-ketoacyl-acyl carrier protein reductase (FabG) interaction. *J. Biol. Chem. 278*, 52935–52943.
37. Horvath, L. A., Sturtevant, J. M., and Prestegard, J. H. (1994) Kinetics and thermodynamics of thermal denaturation in acyl carrier protein. *Protein Sci. 3*, 103–108.
38. Tener, D. M., and Mayo, K. H. (1990) Divalent cation binding to reduced and octanoyl acyl-carrier protein. *Eur. J. Biochem. 189*, 559–565.
39. Altschul, S. F., Madden, T. L., Schaffer, A. A., Zhang, J., Zhang, Z., Miller, W., and Lipman, D. J. (1997) Gapped BLAST and PSI-BLAST: A new generation of protein database search programs. *Nucleic Acids Res. 25*, 3389–3402.
40. Tatusova, T. A., and Madden, T. L. (1999) BLAST 2 Sequences, a new tool for comparing protein and nucleotide sequences. *FEMS Microbiol. Lett. 174*, 247–250.
41. Anderson, M. S., Bulawa, C. E., and Raetz, C. R. H. (1985) The biosynthesis of Gram-negative endotoxin: Formation of lipid A precursors from UDP-GlcNAc in extracts of *Escherichia coli*. *J. Biol. Chem. 260*, 15536–15541.
42. Lee, B. I., and Suh, S. W. (2003) Crystal structure of UDP-*N*-acetylglucosamine acyltransferase from *Helicobacter pylori*. *Proteins 53*, 772–774.
43. Williams, A. H., Immormino, R. M., Gewirth, D. T., and Raetz, C. R. H. (2006) Structure of UDP-N-acetylglucosamine acyltransferase with a bound antibacterial pentadecapeptide. *Proc. Natl. Acad. Sci. U.S.A. 103*, 10877–10882.
44. Malthouse, J. P. (2007) ^{13}C- and ^{1}H-NMR studies of oxyanion and tetrahedral intermediate stabilization by the serine proteinases: Optimizing inhibitor warhead specificity and potency by studying the inhibition of the serine proteinases by peptide-derived chloromethane and glyoxal inhibitors. *Biochem. Soc. Trans. 35*, 566–570.
45. Farazi, T. A., Waksman, G., and Gordon, J. I. (2001) Structures of *Saccharomyces cerevisiae N*-myristoyltransferase with bound myristoylCoA and peptide provide insights about substrate recognition and catalysis. *Biochemistry 40*, 6335–6343.
46. Jaeger, K. E., Dijkstra, B. W., and Reetz, M. T. (1999) Bacterial biocatalysts: Molecular biology, three-dimensional structures, and biotechnological applications of lipases. *Annu. Rev. Microbiol. 53*, 315–351.

47. Pye, V. E., Tingey, A. P., Robson, R. L., and Moody, P. C. (2004) The structure and mechanism of serine acetyltransferase from *Escherichia coli*. *J. Biol. Chem. 279*, 40729–40736.
48. Dotson, G. D., Kaltashov, I. A., Cotter, R. J., and Raetz, C. R. H. (1998) Expression cloning of a *Pseudomonas* gene encoding a hydroxydecanoyl-acyl carrier protein-dependent UDP-GlcNAc acyltransferase. *J. Bacteriol. 180*, 330–337.
49. Wyckoff, T. J. O., Lin, S., Cotter, R. J., Dotson, G. D., and Raetz, C. R. H. (1998) Hydrocarbon rulers in UDP-*N*-acetylglucosamine acyltransferases. *J. Biol. Chem. 273*, 32369–32372.
50. Kim, Y., and Prestegard, J. H. (1989) A dynamic model for the structure of acyl carrier protein in solution. *Biochemistry 28*, 8792–8797.
51. Frederick, A. F., Kay, L. E., and Prestegard, J. H. (1988) Location of divalent ion sites in acyl carrier protein using relaxation perturbed 2D NMR. *FEBS Lett. 238*, 43–48.
52. Davis, I. W., Murray, L. W., Richardson, J. S., and Richardson, D. C. (2004) MOLPROBITY: Structure validation and all-atom contact analysis for nucleic acids and their complexes. *Nucleic Acids Res. 32*, W615–W619.
53. Lovell, S. C., Davis, I. W., Arendall, W. B., III, de Bakker, P. I., Word, J. M., Prisant, M. G., Richardson, J. S., and Richardson, D. C. (2003) Structure validation by Cα geometry: φ, ψ and Cβ deviation. *Proteins 50*, 437–450.

BI800240R